Order-disorder transformation in $Co_{30}Pt_{70}$ alloy: evidence of wetting from the antiphase boundaries

1990 J. Phys.: Condens. Matter 2 3479

(http://iopscience.iop.org/0953-8984/2/15/005)

J. Phys.: Condens. Matter 2 (1990) 3479–3495. Printed in the UK

Order–disorder transformation in $Co_{30}Pt_{70}$ alloy: evidence of wetting from the antiphase boundaries

C Leroux†‡§, A Loiseau‖, M C Cadeville‡, D Broddin† and G Van Tendeloo†

† University of Antwerp, RUCA, Groenenborgerlaan 171, B-2020 Antwerpen, Belgium
‡ Groupe d'Etudes des Matériaux Métalliques, IPCMS (UM CNRS No 380046), 4 rue B Pascal, F-67000 Strasbourg, France
‖ Groupe de Physique du Solide, ONERA, BP 72, F-92320 Chatillon/Bagneux, France

Received 12 June 1989, in final form 5 December 1989

Abstract. A study of the order–disorder $L1_2 \rightarrow A1$ transformation near a congruent point of the Co–Pt phase diagram is presented. This work was performed by combining *in situ* transmission electron microscopy observations, resistivity measurements carried out in conditions near thermodynamic equilibrium and high-resolution imaging on quenched samples. Resistivity measurements display three characteristic temperatures: 994 K, 1020 K and 1032 K. The evolution of the microstructure with temperature at different heating rates was followed in dark field images, until the order–disorder temperature was reached. We found that at temperatures above 994 K ($\simeq$40 K below T_c), the antiphase boundaries (APB) undergo a structural change; the phenomenon becomes more pronounced as the temperature increases. High-resolution images of modified APB show thin layers of disordered phase in the core of these APB. This can be described as a wetting of the antiphase boundaries by the disordered phase. Above 1020 K, up to 1032 K, a second mechanism is superimposed; the disordering occurs through a nucleation, growth and coarsening of disordered regions inside the ordered domains. This nucleation and growth process starts at the beginning of the two-phase region (1020 K). These results are in excellent agreement with those from cluster variation method calculations performed by Kikuchi and Cahn and Finel and co-workers.

1. Introduction

The aim of this work was to investigate under specific conditions the transformation mechanism of the $L1_2$ ordered phase into the A1 (FCC) disordered phase by focusing on the role played by antiphase boundaries. Experimental study of order–disorder transformations has been the subject of numerous papers, especially since electron microscopy methods have become available to observe directly the different variants resulting in the ordered phase from the loss of symmetry at the transformation (for a complete review, see Tanner and Leamy 1974, Reynaud 1982). In the case of the $L1_2$ ordered phase, only translation variants occur, and the interfaces between them are usually called antiphase boundaries (APB). However, most of the studies of order–disorder transformations have been performed on quenched alloys; in particular, the $L1_2 \rightarrow A1$ transformation was investigated in this way in Ni-based alloys (Lasserre *et al*

§ Present address: NCEM, Lawrence Berkeley Lab., University of California, Berkeley, CA 94720, USA.

0953-8984/90/153479 + 17 $03.50

1978, Horton *et al* 1985, Cahn *et al* 1987). In our case, a previous determination of the ordering kinetics in the $L1_2$ ordered phase of the Co–Pt system (Cadeville *et al* 1987), and the fact that Co–Pt alloys are suited for *in situ* electron microscopy experiments, allowed (for the first time, to our knowledge) an *in situ* observation of a disordering process in conditions near the thermodynamic equilibrium. In addition, since resistivity measurements reflect an absolute temperature scale, phenomena observed by *in situ* electron microscopy can be related to the characteristic temperatures indicated by resistivity measurements. Finally, high-resolution images made on quenched samples allow us to analyse on an atomic scale the nature of the structural changes observed. We show that, below the bulk transition temperature, a structural change in APB behaviour occurs and that it can be correlated to a progressive wetting of the APB by the disordered phase. Much attention has recently been devoted to the wetting phenomenon. According to Dietrich (1988): "Wetting phenomena are structural changes of the intrinsic interface between two coexisting phases of matter when a third phase becomes thermodynamically stable. The interphase profile may undergo a transition so that a macroscopic portion of the third phase nucleates at the interface position. This represents a co-operative phenomenon which proliferates the inhomogeneity, which is induced by the interface, into the bulk." Wetting has been predicted in the case of a binary alloy which orders in the $L1_2$ structure using cluster variation method (CVM) calculations by Kikuchi and Cahn, (1979), Sanchez *et al* (1987), Finel *et al* (1990).

First, we present the methodology used to investigate *in situ* this order–disorder transformation (section 2). After giving experimental details of sample preparation and characterisation (section 3), the resistivity curves at different heating rates (section 4) and the electron microscopy observations (section 5) are described and analysed. Finally, the different results are combined and discussed in the framework of a theoretical study of antiphase boundaries in $L1_2$ ordered alloys by means of inhomogeneous CVM calculations in the tetrahedron approximation (section 6).

2. Methodology

Briefly, a first-order transformation such as the $L1_2 \rightarrow A1$ is characterised by: (i) a discontinuity of the long-range order parameter at the order–disorder transition temperature; (ii) the existence of two-phase regions, which separate ordered from disordered regions, except at the congruent point; (iii) the possibility of incoherences between the disordered and the ordered phase, giving rise to elastic strains. Moreover, defects such as antiphase boundaries and interfaces, as well as diffusion, play a key role in the transformation process. The recent determination of the Co–Pt phase diagram (Dahmani 1985, Leroux 1989, Leroux *et al* 1989a) allows a controlled study of the APB role in the transformation process at a given concentration. The concentration of 70% Pt was chosen since it is near to the congruent point, and because of the almost identical lattice parameters in the ordered and disordered phases at this concentration, which means that the order–disorder transformation occurs without elastic strains. Moreover, previous studies of kinetics properties in the $L1_2$ phase (Cadeville *et al* 1987) give, through an extrapolation of the Arrhenius law in the transformation region, a relaxation time of nearly one second, i.e. the order–disorder transformation will not be hampered by atomic diffusion.

The techniques chosen to perform this study were *in situ* diffraction contrast electron microscopy, high-resolution electron microscopy (HREM) and resistivity measurements.

The two-dimensional defects associated with phase transformations are revealed by their contrast in diffraction contrast images; through a direct imaging on an atomic scale by HREM, the nature and density of these two-dimensional defects can be studied. Nevertheless, in a microscope the temperature scale is a relative one, and the information obtained is essentially time limited (4–5 hours). Moreover, experiments are only performed at specific temperatures. Hence, to complete the *in situ* electron microscopy study, we have performed detailed *in situ* resistivity measurements in a furnace at increasing and decreasing temperatures. At each temperature, a measurement point was set up every four minutes, yielding kinetics curves at every temperature. Thus, it is possible to verify the influence of heating rates and temperature steps in the progress of phenomena, and to check whether or not the sample is in an equilibrium state at a given temperature. Besides, resistivity measurements give reliably the temperatures at which events occur.

In situ electron microscopy experiments on a given system are not always possible. The material should: (i) not be contaminated or oxidised in the microscope; (ii) have constituents which do not evaporate in the microscope; (iii) present only a small thermal dilatation; and (iv) have a transformation temperature below roughly 1200 K. The $Co_{30}Pt_{70}$ alloy fulfils all these requirements.

3. Sample preparation and characterisation

The $Co_{30}Pt_{70}$ alloys were prepared by arc melting of pure materials under a purified argon atmosphere, followed by a homogenisation anneal at 1220 K for two days. The samples were rolled into foils of about 0.1 mm in thickness. Strips of a few cm in length, 1 mm in width were cut for resistivity measurements, and discs were punched out of the foils for electron microscopy. All the ordering anneals were performed in quartz tubes under 400 mm of helium. After these ordering anneals, described below, foils for electron microscopy were thinned by ion bombardment.

Samples for *in situ* studies should be ordered as well as possible. To this aim, the following procedure was used: after an anneal in the disordered state (one day at 1050 K) the samples were quenched to retain a large vacancy supersaturation. Samples were then annealed a few degrees below the estimated transition temperature (three days at 995 K) to obtain large ordered domains, and then cooled down to 770 K. The cooling rate was calculated taking into account the atomic relaxation rate ($\tau = \tau_0 \exp(E_A/kT)$, $\tau_0 = 0.4\ 10^{-16}$ s, $E_A = 3.28$ eV) (Cadeville *et al* 1987), so that the degree of long-range order increased during the anneals until the equilibrium state at each temperature was reached. After 13 days at 770 K, the samples were finally quenched to room temperature. This procedure ensures that any modification of the samples during further *in situ* studies is only due to a modification of the ordered state and not to domain growth kinetics. Since HREM can only be performed at room temperature, samples were also annealed at several temperatures (deduced from *in situ* studies) and quenched to room temperature.

The accurate platinum concentration of the samples was defined to within 0.5% by measuring their lattice parameters in the disordered state and by comparing them with data collected by Dahmani (1985) and by Pearson (1964). The final state of order of the samples used for resistivity measurements was checked by measurements of their residual resistivities, since the residual resistivity of an alloy characterises the state of

Table 1. Table giving, for different *in situ* resistivity measurements: the residual resistivity values (ρ_{4K}) from $Co_{30}Pt_{70}$ alloys in their maximal ordered state; the temperature steps (δT) used; the heating rates ($\delta T/\delta t$) in the vicinity of the transformation; and the temperature range (ΔT) covered, at increasing temperature ($\rightarrow$) and at increasing and decreasing temperature ($\leftrightarrow$).

ρ_{4K} ($\mu\Omega$ cm)	δT (K)	$\delta T/\delta t$	ΔT (K)
15.4	5	5 K/1 h	760 $\leftrightarrow$ 1100
14.8	5	5 K/2 h	970 $\leftrightarrow$ 1060
17.5	1	1 K/2 h	940 $\rightarrow$ 1068

order and the concentration of an alloy (Leroux *et al* 1988a). The values obtained are reported in table 1.

4. Resistivity studies

4.1. Experimental procedure

Resistivity measurements were carried out in a furnace, under a He(20% H_2) atmosphere. Two Pt–Pt(10%Rh) thermocouples were used, one to control the furnace temperature and the other, close to the sample, to measure its temperature. Measurements, monitored by a PC were set up every four minutes. At the beginning of the measurements, the alloys were in the ordered state attained by the order anneal described in section 3. An arbitrary heating rate of 5 K h^{-1} was chosen to heat the samples up to the transformation region. As deduced from the relaxation times previously determined (Cadeville *et al* 1987), the samples were at thermodynamic equilibrium from 870 K, in the ordered region. The heating rates were changed before approaching the transformation region: we performed three different runs at heating rates of 5 K/1h, 5 K/2h and 1 K/2h.

4.2. Results

In the case of $Co_{30}Pt_{70}$, the total resistivity is not very sensitive to the order–disorder transformation. An analysis of the $\rho(T)$ curves was previously made in terms of three contributions to the resistivity, namely a residual resistivity term, a phonon term and a spin disorder scattering term (Leroux *et al* 1989a). It shows that the spin disorder scattering decreases as the chemical disorder increases, their respective contributions to the total resistivity being nearly compensated. This explains the very flat variation observed at the order–disorder transition: peculiar features are only visible on the derivative curve. The three derivative curves (figures 1 and 2), made with different heating rates and temperature steps show three singular points, marked 1, 2, 3, at three characteristic temperatures: 994 K, 1020 K and 1032 K.

4.2.1. Heating rate of 5 K/1 h and 5 K/2 h. In the disordered state, the temperature dependence of the resistivity is reversible (Dahmani 1985): then, these two curves (figure 1(*a*), (*b*)), made at increasing and decreasing temperature, give point B (1032 K) as the limit of the reversible region, for measurements set up at increasing temperature.

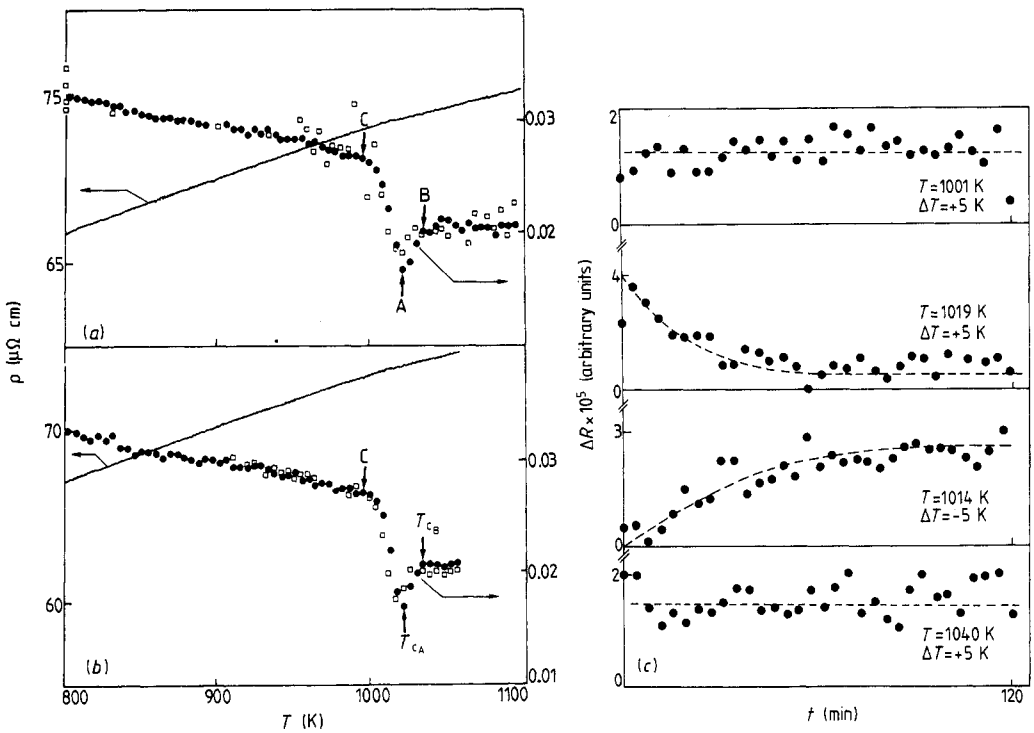

Figure 1. Temperature dependence of the resistivity (full curve) and of its derivative with increasing (●) and decreasing (□) temperature, near the order–disorder transformation of the $Co_{30}Pt_{70}$ alloy. (*a*) Measurements made in steps of 5 K, with a heating rate of 5 K/1h. (*b*) Measurements made in steps of 5 K, with a heating rate of 5 K/2h. (*c*) Time dependence of the resistivity ($\Delta R = R(t) - R(t = 0)$) at four temperatures, showing that kinetics only occur in the $T_{C1} - T_{C2}$ temperature interval. Note the different scales for ΔR.

Electron microscopy studies on samples annealed for one day at various temperatures and quenched show a two-phase region less than 10 K wide (Leroux 1989). Hence, it seems reasonable to attribute point A (1020 K) to the beginning of the two-phase region. Due to the experimental procedure, these two points are determined within an accuracy of 5 K. Moreover, the derivative curves display a weak hysteresis of 5 K, which is characteristic of a first-order transformation. A detailed analysis of the kinetic curves obtained after each temperature step clearly shows in this temperature region measurable time-dependent effects, whose sign is inversed with temperature (figure 1(*c*)). Such effects, whose time constants (some ten minutes) are clearly higher than the atomic relaxation times at these temperatures (nearly one second), are certainly due to a phase transformation. As the observed time constants are smaller than the smallest time spent at each temperature (one hour), this explains why the curves of figure 1(*a*) and (*b*) are similar. Also, these two runs reveal the existence of a third singular point C at 994 K, where the derivative curves starts to decrease with temperature.

4.2.2. Heating rate of 1 K/2 h. The third run was made with a step of 1 K (figure 2). Because of the relative uncertainty of the temperature with respect to the step used, the

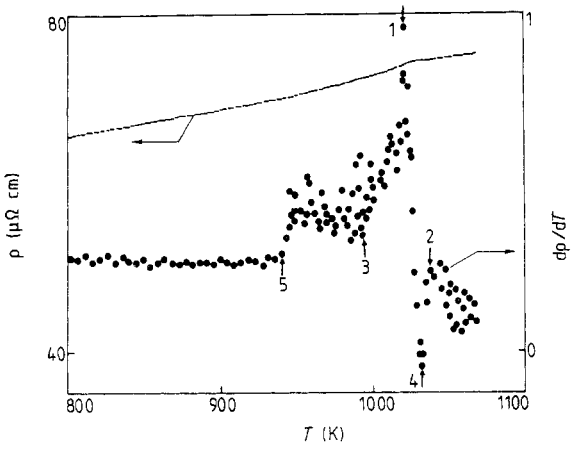

Figure 2. Temperature dependence of the resistivity (full curve) and its derivative (●) with increasing temperature, near the order–disorder transformation of the $Co_{30}Pt_{70}$ alloy. Measurements were made in steps of 1 K, with a heating rate of 1 K/2h.

derivative curve presents fluctuations. Nevertheless, in this curve too, three characteristic points appear at the same temperature as before. The singular point marked 5 originates from a change in the heating rate. In this run, point 3 corresponds to the beginning of an abrupt increase of $d\rho/dT$, instead of the decrease observed previously (figure 1). A careful examination of the resistivity time dependence shows that from about 994 K, one observes a time-linear increase, this effect becoming increasingly important until reaching point 2. This is the origin of the different behaviour displayed by figures 1 and 2 between 994 K and 1020 K. Beyond 1020 K, probably the same effect as in the first two runs occurs, i.e., a decrease in the resistivity associated with the phase transformation. Point 4, which is only observed in this run, would be due to a compensation between both effects.

5. Electron microscopy studies

5.1. Definition and electron microscopy characterisation of antiphase boundaries

Figure 3(*a*) recalls the stucture of the $L1_2$ (AB_3) ordered phase. It contains four different atomic sites which are those of the underlying FCC lattice. This structure is usually described by four interpenetrating single cubic sublattices, labelled I, II, III, IV. With regards to the structure of the A1 disordered phase, $L1_2$ is characterised by a loss of the $a/2\langle 110\rangle$-type translation. Owing to the symmetry breaking between A1 and $L1_2$, the $L1_2$ structure grows coherently from the disordered state in four different translation variants, depending on the sublattice occupations. Each ordered domain or translation variant can be labelled I, II, III, IV depending on which sublattice is occupied by the minority A atoms. Antiphase boundaries form wherever different translation variants make contact. An antiphase boundary is characterised by (i) the contact plane between two translation variants and (ii) the displacement vector, which joins the sublattice sites occupied by A atoms in each domain separated by the APB. In the $L1_2$ structure, there are three displacement vectors:

$$\boldsymbol{R}_1 = \tfrac{1}{2}[011] \qquad \boldsymbol{R}_2 = \tfrac{1}{2}[101] \qquad \boldsymbol{R}_3 = \tfrac{1}{2}[110].$$

Figure 3(*b*) is a sketch of different kinds of APB between ordered domains, in a

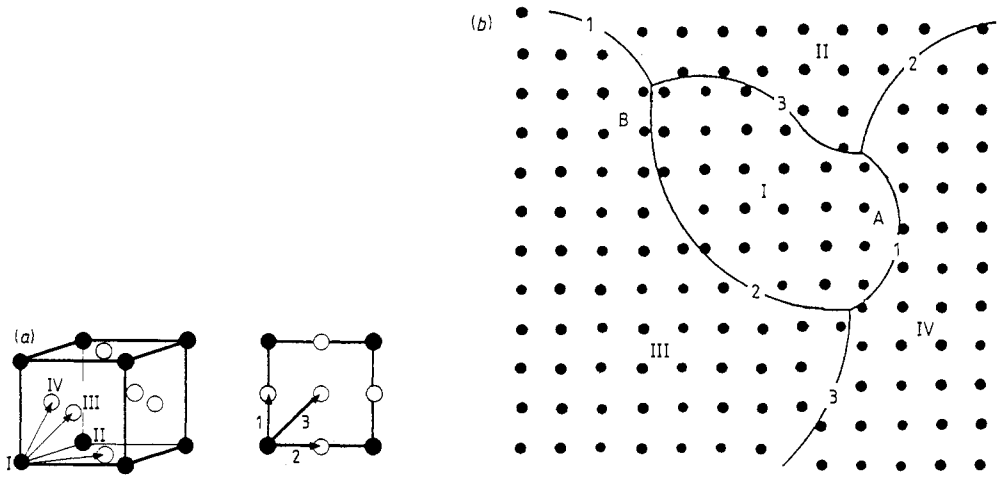

Figure 3. (*a*) The $L1_2$-type structure, together with its projection along a [001] axis. The three types of displacement vectors, labelled 1, 2, 3, together with the different sublattices I, II, III, IV, are indicated. (*b*) [001] projected sketch of different kinds of APB, where only the minority atoms are indicated. A and B correspond respectively to locally conservative APB and non-conservative APB.

Table 2. Contrast in dark field images made using superstructures of a [001] zone for the three types of antiphase boundaries of the $L1_2$ structure.

	(100)	(010)	(110)
$\boldsymbol{R}_1 = \frac{1}{2}[011]$	0	π	π
$\boldsymbol{R}_2 = \frac{1}{2}[101]$	π	0	π
$\boldsymbol{R}_3 = \frac{1}{2}[110]$	π	π	0

projection along a [001] axis, for which only minority atoms are represented. Different situations arise at the APB, depending on whether the concentration AB_3 is locally maintained (conservative APB) or not (non-conservative APB). In the second case, the displacement vector never lies in the APB plane.

The displacement vector $\boldsymbol{R}$ can easily be determined in diffraction contrast electron microscopy. Generally, a defect plane characterised by a displacement vector $\boldsymbol{R}$ introduces a phase shift in the transmitted and scattered waves. When a two-beam situation is realised, i.e., when there is in addition to the transmitted beam only one diffracted beam characterised by a diffraction vector, $\boldsymbol{g}$, the phase shift is $\alpha = 2\pi \boldsymbol{g} \cdot \boldsymbol{R}$. When $\boldsymbol{g}$ is such that $\alpha \neq 2\pi n$, the fault will be imaged by a fringe contrast (called α-fringes). If $\alpha = 2\pi n$, the fault will be out of contrast. Since for the $L1_2$ structure the displacement vector is of the form $\boldsymbol{R} = \frac{1}{2}$ (lattice vector), the phase shift only adopts two values: 0 and π, the latter value being obtained for the superstructure reflections only. Owing to this particularity, the displacement vector can be determined by comparing APB contrast in three dark field images formed with the superstructure reflections (100), (010) and (110) of a [001] zone axis. A given APB is out of contrast in only one of these three dark field images and in contrast in the two others, as shown in table 2. An example of APB

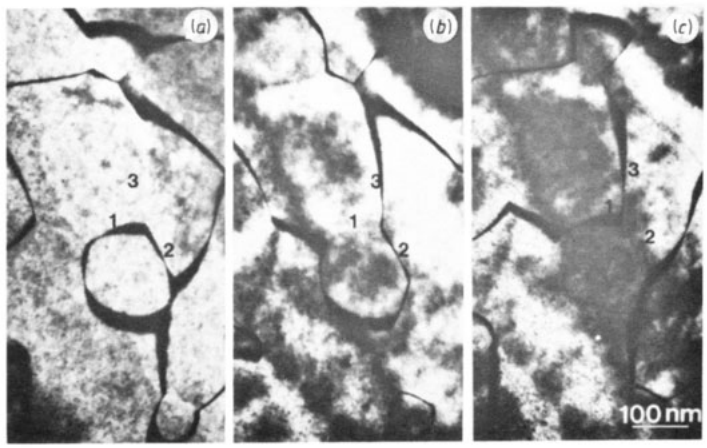

Figure 4. Two-beam dark field images of a typical $L1_2$ microstructure using (*a*) (110), (*b*) (100) and (*c*) (010) reflections.

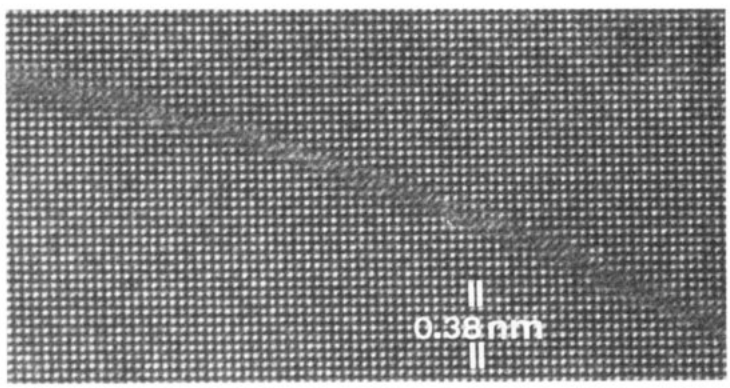

Figure 5. [001] high-resolution image showing a perfect APB in the $L1_2$ structure, with a displacement vector $\boldsymbol{R}_3 = \frac{1}{2}[110]$.

identification is given in figure 4 which illustrates the microstructure of the $L1_2$ ordered phase observed in a $Co_{30}Pt_{70}$ alloy, slowly cooled and annealed for 13 days at 770 K. The different kinds of APB are labelled 1, 2, 3 according to table 2. Since APB contrast changes with the superstructure reflection used, the three dark field images reveal different but complementary information.

In high-resolution images made with an aperture including several basic as well as superstructure reflections up to (220), the $L1_2$ structure appears, in a projection along [001], as a square pattern of bright dots separated by a distance equal to the lattice parameter of the structure. These bright dots correspond to minority atom columns along the projection direction, as shown by computer simulations (Van Dyck *et al* 1982). Figure 5 is a high-resolution image of an APB in a $Co_{30}Pt_{70}$ alloy, slowly cooled and annealed for 13 days at 770 K. The bright dots correspond to Co atom columns and the APB is directly visualised as a shift of the rows of bright dots from one side of the boundary to the other; the displacement vector in this case is $\boldsymbol{R}_3 = \frac{1}{2}[110]$.

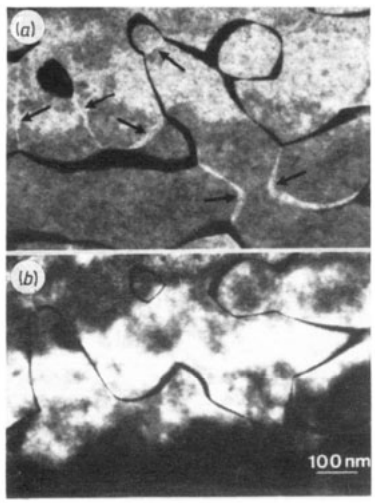

Figure 6. APB in the initial stage of the disordering process, showing perfect extinction rules: two-beam dark field images at room temperature using (*a*) (110) and (*b*) (100) reflections.

5.2. Heating procedure

Thermal stability in the heating holder of the electron microscope is rapidly attained (in a few minutes), which allows fast changes in temperature. The thermocouple indicates only the temperature of the heating element so that the temperature of the sample is not precisely known. During an experiment, the local temperature can be significantly increased by the electron beam; this effect depends on the intensity of the beam and on the thickness of the region of interest. Thus special care was taken to ensure reproducible observations by, (i) selecting areas of constant thickness, and (ii) working under constant illumination conditions—same filament current, condenser apertures and spot size. Under those conditions, a first *in situ* disordering experiment was performed to determine the *in situ* transition temperature T_D and to calibrate the temperatures with regard to it. The procedure used to observe the disordering process was as follows: the temperature was progressively increased up to $T_D - 40$ K (in two hours), so that nearly all the different thermal expansions had taken place. The temperature was then increased by steps of half an hour at $T_D - 40$ K, $T_D - 17$ K, $T_D - 9$ K and finally at T_D; this heating rate is slow enough to reach equilibrium at these temperatures, with regard to the atomic relaxation rate (see section 3). Evolution of microstructure with temperature and time was followed in the dark (1 1 0) field mode; the nature of the APB was investigated by rapidly changing the diffraction vector. The sample was therefore oriented near a [001] zone axis. The experiments were recorded and assembled on film (Leroux and Loiseau 1988).

5.3. Description of the disordering process

5.3.1. Microstructure at room temperature. Figure 6 corresponds to the microstructure in the initial stage of our *in situ* study, as obtained after the ordering process described in section 3. Arrows indicate the APB of type 3, which are out of contrast in the (110) dark field of figure 6(*b*). In order to localise them in this dark field image a slight deviation from the two-beam orientation conditions was made, so that they appear with a soft white contrast. The APB are mostly inclined with respect to the electron beam and

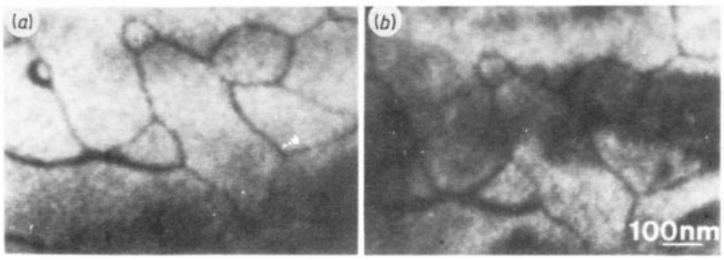

Figure 7. APB at $T_D - 17$ K: a slight contrast is seen for APBs previously out of contrast; dark field images made at this temperature after 3 min, using (*a*) (110) and (*b*) (100) reflections.

therefore appear with different widths. The straightest APB have an apparent contrast width of 1.5 nm.

5.3.2. Microstructure at $T_D - 40$ K. At $T_D - 40$ K, the APB's contrast is slightly modified. In the (110) dark field, the APB of type 3, which were out of contrast before reaching this temperature, appear with a residual contrast, although weaker than the contrast of APB of type 1 and 2. This modification of the APB contrast becomes more pronounced at $T_D - 17$ K.

5.3.3. Microstructure at $T_D - 17$ K. At $T_D - 17$ K the APB contrast is rapidly altered, as shown in figure 7, which gives the APB's contrast after three minutes at this temperature. When changing the diffraction vector, one can see that the same alteration occurs for each type of APB (figure 7(*a*), (*b*)). So, in spite of a contrast modification, APBs can still be distinguished. At the same time, all the APB's contours are smoothed, and APB contrast seems more uniform: APBs tend to be edge on. This modification in orientation may be due to an interaction of the APB with the thin foil surface. Furthermore, APBs edge on seem to have an apparent width of about 10 nm. These phenomena occur very rapidly and do not change noticeably after 25 minutes.

5.3.4. Microstructure at $T_D - 9$ K. The changes initiated at lower temperatures become more pronounced. All the APBs (type 1, 2 or 3) are seen with the same dark contrast for all superstructure reflections used, proving the presence of a disordered zone, and with a constant apparent width. This width increases with time from 10 nm to 40 nm after 25 minutes (Figure 8(*a–d*)). Besides, a mottled contrast inside the ordered domains becomes significant and increases with time, due to a homogeneous nucleation of the disordered phase. The intensity of the superstructure reflections simultaneously decreases with time.

5.3.5. Microstructure at T_D. The sample is completely disordered after three minutes at this temperature, as shown in figure 9. Inside the ordered domains, germs of the disordered phase nucleate and grow until the ordered phase disappears; the mottled character of the contrast increases and the diffracted intensity decreases. At the same time, the apparent width of the APB broadens up to 60 nm, but it becomes increasingly difficult to distinguish between them and the domains. Nevertheless, the APB width is finite until the final stage of the disordering process.

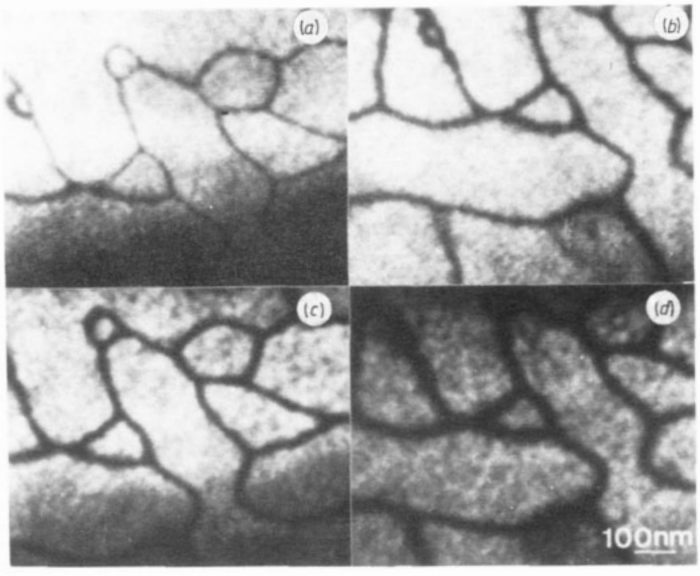

Figure 8. APB at $T_D - 9$ K, all having the same wide dark contrast: (110) dark field images, made after (*a*) 1 min, (*b*) 12 min, (*c*) 18 min and (*d*) 24 min.

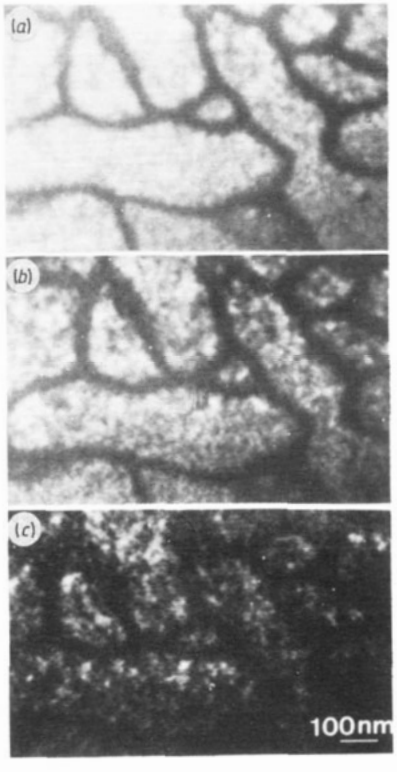

Figure 9. APB at T_D: (110) dark field images, made after (*a*) 1 min, (*b*) 2 min and (*c*) 3 min.

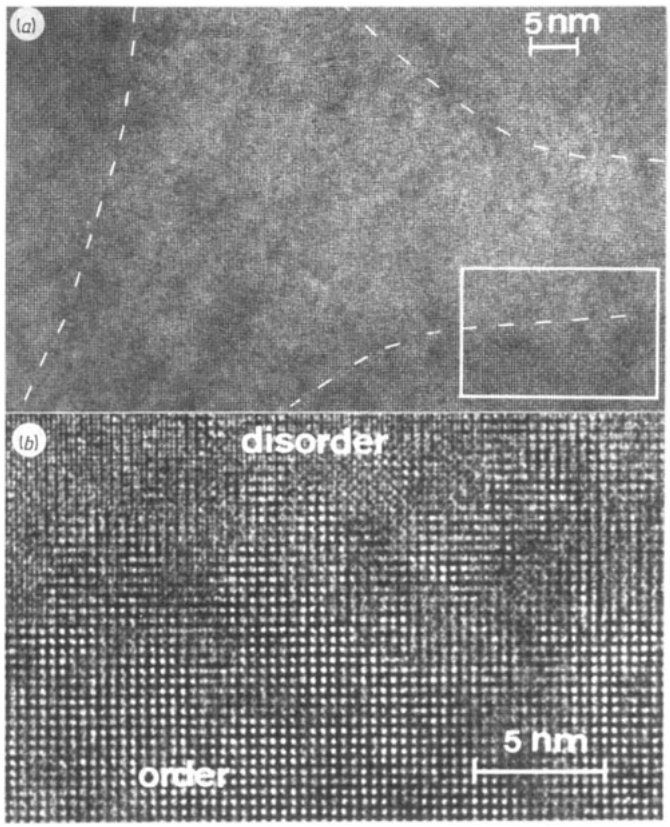

Figure 10. (*a*) High-resolution image of antiphase domains separated by a thick layer of disordered phase. An aperture including the fundamental reflections has been used. The occurrence of short-range order in the disordered phase can probably be related to the quench. (*b*) Higher magnification of an order–disorder interface: note its diffuse character.

5.4. Analysis of the disordering process

The nucleation of the disordered phase at $T_D - 9$ K indicates that the order–disorder transformation in the bulk has already begun at this temperature. Hence this temperature can be roughly considered as the lower limit of the two-phase region, T_{C1} (Leroux *et al* 1990), which is approximately equal to 1020 K, as determined by resistivity measurements. Since the alloy is completely disordered in a few minutes, the temperature we labelled T_D should be higher than T_{C2}, i.e., the upper limit of the two-phase region. The extension of this can be estimated to be about 5 K. At $T_D - 9$ K, the different APBs can no longer be distinguished from each other and their contrast is that of a disordered layer several nm thick. HREM of a $Co_{30}Pt_{70}$ alloy annealed for one day at 1023 K and quenched shows three $L1_2$ domains in antiphase separated by a thick layer of disordered phase (figure 10(*a*)): each APB is split into two order–disorder interfaces. Notice that these interfaces are not well defined and seem to be fractal-like (figure 10(*b*)). The increase in the APB's apparent width with the annealing time indicates an

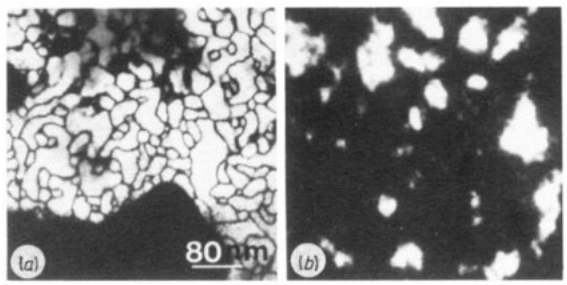

Figure 11. Disordering process of a sample initially ordered with small domains: (110) dark field images made at (*a*) room temperature and (*b*) high temperature.

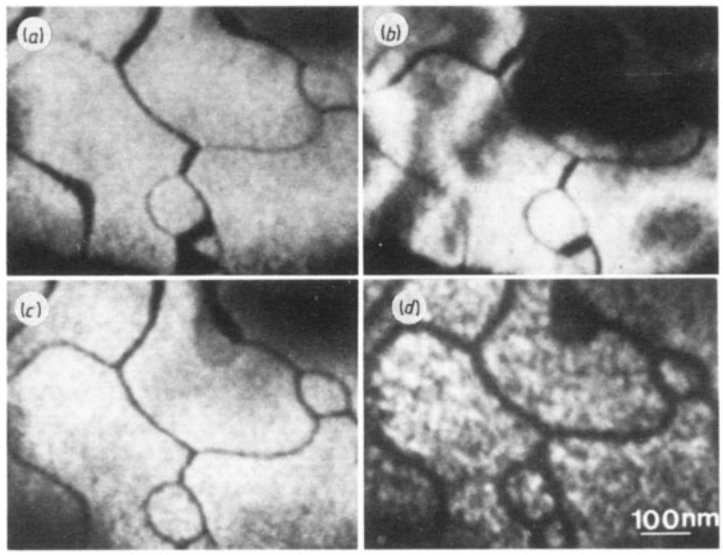

Figure 12. Fast disordering process of a $Co_{30}Pt_{70}$ sample initially ordered for one day at 1000 K and quenched: dark field images at $T_D - 40$ K using (*a*) (110) and (*b*) (100) reflections, and (110) dark field images at (*c*) $T_D - 14$ K and (*d*) T_D.

increase of the disorder. On the other hand, the complete transformation does not occur through this mechanism. Its importance depends on the density of the APB, i.e., the size of the ordered domains, and of the heating rate. The first point is illustrated by figure 11: the initial microstructure consists of many little ordered domains (figure 11(*a*)). As the temperature increases, the domains grow to a slight extent. The transformation occurs through a growth of the disordered phase between the ordered domains and in the two-phase region, there only remain some ordered domains in a disordered matrix (figure 11(*b*)). In another study of the disordering process, made by steps of ten minutes instead of 30 minutes, the APBs width remains smaller in the two-phase region and the disorder appears principally through a nucleation and growth process in the ordered domains (figure 12). This shows that the kinetics of the two processes, (broadening of the APB and nucleation in the ordered domains) are in competition during the transformation.

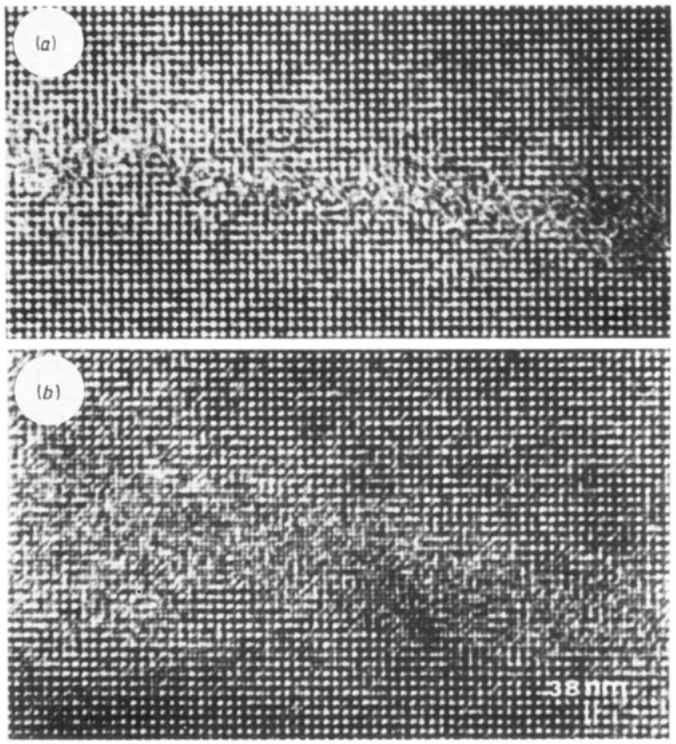

Figure 13. High resolution of wet antiphase boundaries, in a projection along [001]. An aperture including the fundamental reflections has been used. (*a*) Initial stage of the wetting phenomenon: roughly four atomic planes are disordered. (*b*) Further stage of the wetting phenomenon: the FCC pattern inside the APB appears clearly.

Before the transformation in the bulk starts, the APBs undergo a structural change in the ordered phase: at $T_D - 40$ K, and even more at $T_D - 17$ K, the APBs can no longer be considered as perfect thin walls separating $L1_2$ ordered domains. High-resolution imaging of annealed and quenched samples reveals the existence of a few disordered planes in the core of these APBs (figure 13). At each side of the boundaries, the $L1_2$ domains in antiphase appear as a square pattern of bright dots corresponding to Co atom columns. The boundaries appear diffuse with a lower contrast than the ordered domains; the same type of diffuse contrast as in figure 13(*a*) has been previously observed for APBs in Cu_3Pd alloys and related to disordered planes (Broddin *et al* 1988). Moreover, in the central part of the boundary in figure 13(*b*) one can distinguish a square pattern of grey dots with a periodicity half that of the $L1_2$ pattern, which is characteristic of the disordered FCC structure. Such a transformation of the APB, occurring at a temperature below the bulk critical temperature, can be described as the wetting of the APB by the disordered phase.

Note that studies of the ordering process at two different temperatures were also performed (Leroux *et al* 1988b), confirming the expected $t^{1/2}$ kinetic law for APB motion (Allen and Cahn 1979; see also references in Leroux 1989). This ordering process occurs in the same way as the disordered process. When lowering the temperature, the ordered germs nucleate into the disordered matrix, grow and coalesce if they are in phase. If

they are in antiphase, the disorder between them slowly vanishes, giving rise in the end to antiphase boundaries.

6. Discussion and conclusion

By adding resistivity results, which give reliable temperatures where phenomena occur, and TEM observations of these phenomena, it appears that two order–disorder transformation regions can be defined.

6.1. Between 994 K and 1020 K

The APBs are shown to be diffuse and are spread out over a few disordered planes. The number of disordered planes becomes greater with increasing temperature. This evolution below the coexistence field can be related to a progressive wetting by the disordered phase of the APB; an APB, which initially separated two ordered domains, slowly transforms into two interfaces in between which a disordered layer is generated. Kinetic effects with very large time constants are observed.

6.2. Between 1020 K and 1032 ± 5 K

When the temperature of coexistence is reached, APBs transform into thick layers of disordered phase. The two-phase field is also characterised by a nucleation of disordered regions into the ordered domains. At 1032 ± 5 K, the apparent width of the APB remains finite. Kinetic effects related to the transformation in bulk are observed in this region.

The two results—(i) wetting transition of the APB into the ordered phase, and (ii) evolution of the APB's width with temperature—were previously predicted by Kikuchi and Cahn in the frame of CVM calculations (Kikuchi and Cahn 1979). These authors have investigated the evolution with temperature of antiphase boundaries and of order–disorder interfaces, close to or at the congruent point of Cu_3Au, ordered in the $L1_2$ structure. Their model only includes first-neighbour interactions (tetrahedron approximation), which implies in particular that the free energy vanishes for conservative APBs in (100). Therefore, the authors considered non-conservative APBs in (100) planes. The consideration of non-conservative (100) APBs does not restrict the results of the model, since further calculations made by Sanchez *et al* (1987) on (111) APBs lead to similar conclusions. The results of Kikuchi and Cahn's calculations are expressed in terms of antiphase boundary profiles, which correspond to variations of the sublattice occupation by minority atoms with the increasing number of successive (100) planes. Below the congruent point, the structure of the APB is modified and the disordered phase appears. There is an equilibrium width for the APB at each temperature. At the congruent point, an antiphase boundary consists of two interfaces between ordered and disordered phase (figure 14).

Apparently, there is a good qualitative agreement between the present observations on the $L1_2 \rightarrow A1$ transformation and the predictions of the model of Kikuchi and Cahn. The first-neighbour interactions approximation however does not hold for the $Co_{30}Pt_{70}$ alloy, where interactions of higher order are to be expected.

Recently, the behaviour of the same antiphase boundaries as in Kikuchi and Cahn's model was investigated by more accurate inhomogeneous CVM calculations in the tetra-

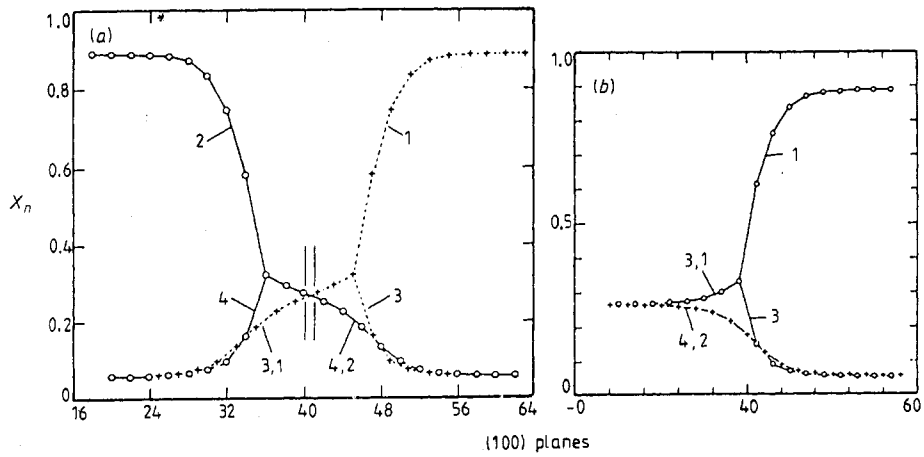

Figure 14. (*a*) Antiphase boundary and (*b*) interface profiles, at the congruent point (Kikuchi and Cahn 1979). The APB, separating initially two ordered domains, has become two order–disorder interfaces, (the disordered phase is characterised by the same occupation probability for the four sublattices).

hedron approximation (Finel *et al* 1990). The authors show that even in a situation where the ordered phase is described by a three-dimensional order parameter, the width of an APB has a logarithmic behaviour as the temperature increases up to T_C, and thus complete wetting (i.e., divergence of the APB width) occurs. Although we found that the width of the disordered layer remains finite as the disordering proceeds, the observed behaviour can be considered as an interfacial wetting, since the width of the disordered layer has become macroscopic and comparable to the domain size. Other experiments with more temperature steps and with a more quantitative analysis of the APB width's evolution should be performed to reflect an eventual divergence. When quantifying the APB's width, several factors have to be taken into account.

(i) On quenched samples one cannot avoid the fact that ordering takes place during cooling. In figure 10 (see earlier), it is clear that the 'disordered' area shows ordered nuclei, which are most likely generated during the quench. It is therefore probable that the same phenomenon occurs at the order–disorder interface, leading to a smaller 'disorder-width' than with *in situ* samples.

(ii) The imaging mode in high resolution and in conventional microscopy is different and the apparent APB widths cannot simply be compared—for a perfect APB imaged edge on, HREM will indicate a single defect plane and conventional microscopy always indicates a minimum width, depending on the aperture.

(iii) Since APBs in $Co_{30}Pt_{70}$ are isotropic, many inclined APBs are observed, and it is not trivial to differentiate between one inclined but perfect APB and an APB decorated by a disordered layer.

The finite width even at T_D could be related to the fact that 70% Pt does not exactly correspond to the concentration of the congruent point and thus one has to go through a two-phase region, where the disorder transformation occurs through a nucleation and growth process. One should also search for the exact congruent point in order to

see whether the whole transformation can proceed from APBs, without the need of a nucleation and growth process.

To summarise, the wetting of APB in $Co_{30}Pt_{70}$ has been shown to take place about 40 K below the coexistence region. The order–disorder transformation occurs through two mechanisms, wetting from the APB into the ordered phase, and nucleation and growth of the disordered phase inside ordered domains, the latter starting at the beginning of the two-phase regime. The relative importance of the two mechanisms depends on the initial state and on the heating rate.

Acknowledgments

We are grateful to A Finel and F Ducastelle for stimulating discussions. Ph Vennegues is acknowledged for the preparation of the samples. One of us (CL) is indebted to the EEC for financial support (SC1–0113).

References

Allen S M and Cahn J W 1979 *Acta Metall.* **27** 1085
Broddin D, Van Tendeloo G, Van Landuyt J, Amelinckx S and Loiseau A 1988 *Phil. Mag.* B **57** 31
Cadeville M C, Leroux C, Pierron-Bohnes V and Dahmani C E 1987 *Proceedings in Physics* vol 10, ed C Janot *et al* (Berlin: Springer) p 78
Cahn R W, Siemers P A and Hall E L 1987 *Acta Metall.* **35** 2753
Dahmani C E 1985 *Thesis* L Pasteur University, Strasbourg
Dietrich S 1988 *Phase Transitions and Critical Phenomena* vol 12, ed C Domb and J Lebowitz (New York: Academic)
Finel A, Mazauric V and Ducastelle F 1990 *Proc. Inc. Conf. on Interfaces and Grain Boundaries (Paris, 1989)*; *J. Physique Coll.* at press
Horton J A, Dasgupta A and Liu C T 1985 *High Temperature Ordered Intermetallic Alloys* vol 39, ed C C Koch *et al* (Pittsburgh, PA: Mater. Res. Soc.) p 109
Kikuchi R and Cahn J W 1979 *Acta Metall.* **24** 1337
Lasserre A, Reynaud F and Coulomb P 1978 *Scr. Metall.* **12** 715
Leroux C 1989 *Thesis* L Pasteur University, Strasbourg
Leroux C, Cadeville M C and Kozubsky R 1989a *J. Phys.: Condens. Matter* **1** 6403
Leroux C, Cadeville M C, Pierron-Bohnes V, Inden G and Hinz F 1988a *J. Phys. F: Met. Phys.* **18** 2033
Leroux C and Loiseau A 1988 *In situ electron microscopy study of the $L1_2 \leftrightarrow A1$ transition in $Co_{30}Pt_{70}$* film ONERA No 1202
Leroux C, Loiseau A, Cadeville M C and Ducastelle F 1990 *Europhys. Lett.* at press
Leroux C, Loiseau A and Cadeville M C 1988b *EUREM 88 (Inst. Phys. Conf. Ser. 93)* vol 2 (Bristol: Institute of Physics) ch 13, p 485
Pearson W 1964 *Handbook of Lattice Spacings and Structure of Metals and Alloys* (New York: Pergamon)
Reynaud F 1982 *Phys. Status Solidi* a **72** 11
Sanchez J M, Eng S, Wu Y P and Tien J K 1987 *Mater. Res. Soc. Symp. Proc.* vol 81, p 57
Tanner L E and Leamy H J 1974 *Proc. Int. Symp. of Order–Disorder Transitions in Alloys (Tülingen, Federal Republic of Germany, 1973)* ed. H Warlimont (Berlin: Springer) p 181
Van Dyck D, Van Tendeloo G and Amelinckx S 1982 *Ultramicroscopy* **10** 263
—— 1984 *Ultramicroscopy* **15** 357